IOP Publishing Journal of Geophysics and Engineering
J. Geophys. Eng. **13** (2016) 622–633 doi:10.1088/1742-2132/13/4/622

Migration velocity analysis using residual diffraction moveout: a real-data example

Jaime A C Gonzalez[1,3], José J S de Figueiredo[1,3], Tiago A Coimbra[2,3], Jörg Schleicher[2,3] and Amélia Novais[2,3]

[1] Faculty of Geophysics, Federal University of Pará (UFPA), Petrophysics and Rock Physics Laboratory—Prof Dr Om Prakash Verma, Belém (PA), Brazil
[2] Institute of Mathematics, Statistics, and Scientific Computing (IMECC), University of Campinas (Unicamp), 13083-859, Campinas (SP), Brazil
[3] National Institute for Petroleum Geophysics (INCT-GP), Brazil

E-mail: jadsomjose@gmail.com

Received 1 February 2016, revised 19 May 2016
Accepted for publication 23 June 2016
Published 20 July 2016

Abstract

Unfocused seismic diffraction events carry direct information about errors in the migration-velocity model. The residual-diffraction-moveout (RDM) migration-velocity-analysis (MVA) method is a recent technique that extracts this information by means of adjusting ellipses or hyperbolas to uncollapsed migrated diffractions. In this paper, we apply this method, which has been tested so far only on synthetic data, to a real data set from the Viking Graben. After application of a plane-wave-destruction (PWD) filter to attenuate the reflected energy, the diffractions in the real data become interpretable and can be used for the RDM method. Our analysis demonstrates that the reflections need not be completely removed for this purpose. Beyond the need to identify and select diffraction events in post-stack migrated sections in the depth domain, the method has a very low computational cost and processing time. To reach an acceptable velocity model of comparable quality as one obtained with common-midpoint (CMP) processing, only two iterations were necessary.

Keywords: diffraction imaging, velocity analysis, local slope, seismic imaging

(Some figures may appear in colour only in the online journal)

Introduction

When seismic waves interact with small structures in the subsurface of the earth (e.g. faults, fractures, channels, tips, and rough edges of salt bodies), waves are scattered in many directions. The typical scattered signatures, known as diffractions, have been investigated for a long time with the purpose of understanding the signatures and how they might be used in seismic processing. The special features exhibited by diffraction signatures (hyperbolas) have been particularly useful in the application of diffractions in velocity analysis (Sava *et al* 2005, Fomel *et al* 2007, Novais *et al* 2008, Landa *et al* 2008, Coimbra *et al* 2013), super-resolution (Khaidukov *et al* 2004), linear fracture imaging (Alonaizi *et al* 2013) and CO_2 time-lapse monitoring (Alonaizi *et al* 2014).

Diffractions are particularly useful for velocity analysis, because they carry immediate velocity information that does not depend on data redundancy. Coimbra *et al* (2013) presented a cheap migration-velocity-analysis (MVA) method to use the residual moveout of unfocused diffraction events in order to locally improve the velocity model. This residual-diffraction-moveout (RDM) method is based on adjusting ellipses or hyperbolas to the unfocused diffraction events after migration. The half-axes of these ellipses or hyperbolas provide information on how to locally update the velocity model. Coimbra *et al* (2013) were able to construct a good velocity model for the Sigsbee2B data set from the residual moveout of a relatively small number of diffractions.

However, because seismic waves reflected at continuous boundaries carry much more energy, generally most time in conventional processing of real data is spent on reflection events. Diffraction events are often almost invisible due to their weak seismic energy and are then considered noise in seismic processing. In such cases, conventional processing

distorts the shape of a diffraction. Then, the true information about the structure carried by this wave type (Zhang 2004) is lost. Therefore, it is recommendable to separate diffractions from reflections before any further analysis.

Many studies have been dedicated to separating diffractions from reflections and using their signatures in seismic processing. Khaidukov *et al* (2004) proposed to mute the reflections by focusing and defocusing the residual wave-field in a shot gather that contains mostly shot diffractions. Dell and Gajewski (2011) and Asgedom *et al* (2011) used the common reflection surface (CRS) concept to suppress the reflections, through the selection of an appropriate stacking surface for diffractions based on a coherency measurement named MUSIC. Klokov and Fomel (2013) used Radon transform to separate diffractions from reflections in the dip-angle domain. Liu *et al* (2013) proposed the singular spectrum analysis (SSA) method, which removes diffractions from the full wave field by taking advantage of the difference between the kinematic and dynamic properties of reflections and diffractions. Using the difference of these properties, Landa *et al* (1987) and Landa and Keydar (1998) developed methods to locate the diffraction points in the time domain and de Figueiredo *et al* (2013) in the depth domain.

In this work, we apply the RDM velocity-analysis method of Coimbra *et al* (2013) to a real data set from the Viking Graben. Since the diffractions are rather weak in these data, we used a rudimentary diffraction separator to enhance them. For this purpose, we implemented a diffraction filter based on plane-wave destruction (PWD) according to Claerbout (1992) and Fomel (2009) together with the local slope approach developed by Schleicher *et al* (2009). These authors use the local event slopes to carry out the PWD with a simple correction to the linear version. The idea is based on the fact that the slope's inverse can be extracted from the data in a fully analogous way. Combining the information of the slope and its inverse can yield a simple but effective correction to the local slope. To attenuate the reflections and enhance the diffractions, we use the smooth background variations of the slope.

After diffraction filtering, we apply the RDM velocity analysis of Coimbra *et al* (2013) to the identifiable diffractions. Although the RMD technique was originally developed for zero-offset data, we apply it to near-offset data. The resulting error reduces after a few iterations. The number of necessary iterations depends on the complexity of the data set. Finally, we compare the results, i.e. the velocity model and migrated seismic image (in the time and depth domains) to those obtained by conventional seismic processing.

Methodology

Let us start with a brief summary of the residual diffraction moveout (RDM) migration-velocity analysis. In order to enhance the visibility of diffractions in the data, we make use of a plane-wave-destruction (PWD) filter to separate diffractions from reflections in near offset sections before the application of the RDM method. After separation, we use the residual moveout of an incorrectly migrated diffraction event in the depth domain to update of velocity model. Although the theory is developed for zero-offset sections, we assume that the error produced by the application to a near-offset section is corrected along the processing after some iterations.

PWD filter and local slope

According to Claerbout (1992), plane-wave destruction (PWD) can be used to attenuate almost planar events associated with reflections. In Claerbout (1992), PWD is defined by means of the local plane-wave differential equation given by

$$\frac{\partial P}{\partial x} + \sigma \frac{\partial P}{\partial t} = 0, \tag{1}$$

where P is the wavefield that depends on offset x, time t, and the local-slope parameter σ. Thus, according to the equation (1), to implement a PWD filter, we need to estimate σ.

If we attribute smooth variations of the local-slope parameter σ to reflection events and stronger lateral variations to diffraction events, we can distinguish both kinds of coherent events. Under this assumption, we can apply PWD by means of equation (1) only to those points in the seismic image with little lateral variation. In this way, the residual of equation (1) is predominantly a diffraction seismic image.

To determine parameter σ, there are several variations to the method described by Claerbout (1992), who suggested an iterative method to minimize the residual, i.e. data not satisfying equation (1). Fomel (2009) implemented an all pass filter to find a similar solution using a frequency-domain version of equation (1). However, this process required high computational resources. Therefore, we rely on the PWD version of Schleicher *et al* (2009) to estimate σ. It uses not only the quadratic residual $R(\sigma)$ of equation (1), given by

$$R(\sigma) = \sum_{i,j}^{W} \left(\frac{\partial P(x_i, t_j)}{\partial x} + \sigma \frac{\partial P(x_i, t_j)}{\partial t} \right)^2, \tag{2}$$

but also the complementary residual $\tilde{R}(q)$ for its inverse,

$$\tilde{R}(q) = \sum_{i,j}^{W} \left(q \frac{\partial P(x_i, t_j)}{\partial x} + \frac{\partial P(x_i, t_j)}{\partial t} \right)^2, \tag{3}$$

where $q = 1/\sigma$. Here, W is the size of the window selected around point (x_i, t_j). Equations (2) and (3) can be combined to give a simple and effective correction of the local slope. According to Schleicher *et al* (2009), the total-least-squares solution to this problem is given by

$$\langle \sigma \rangle_E = S \sqrt{\frac{\sum_{i,j}^{W} \left(\frac{\partial P(x_i, t_j)}{\partial x} \right)^2}{\sum_{i,j}^{W} \left(\frac{\partial P(x_i, t_j)}{\partial t} \right)^2}}, \tag{4}$$

where S is defined as

$$S = -\mathrm{sgn}\left(\sum_{i,j}^{W} \left(\frac{\partial P(x_i, t_j)}{\partial x} \right) \left(\frac{\partial P(x_i, t_j)}{\partial t} \right) \right). \tag{5}$$

Equation (4) minimizes the error of the total-least-squares solution of equations (2) and (3).

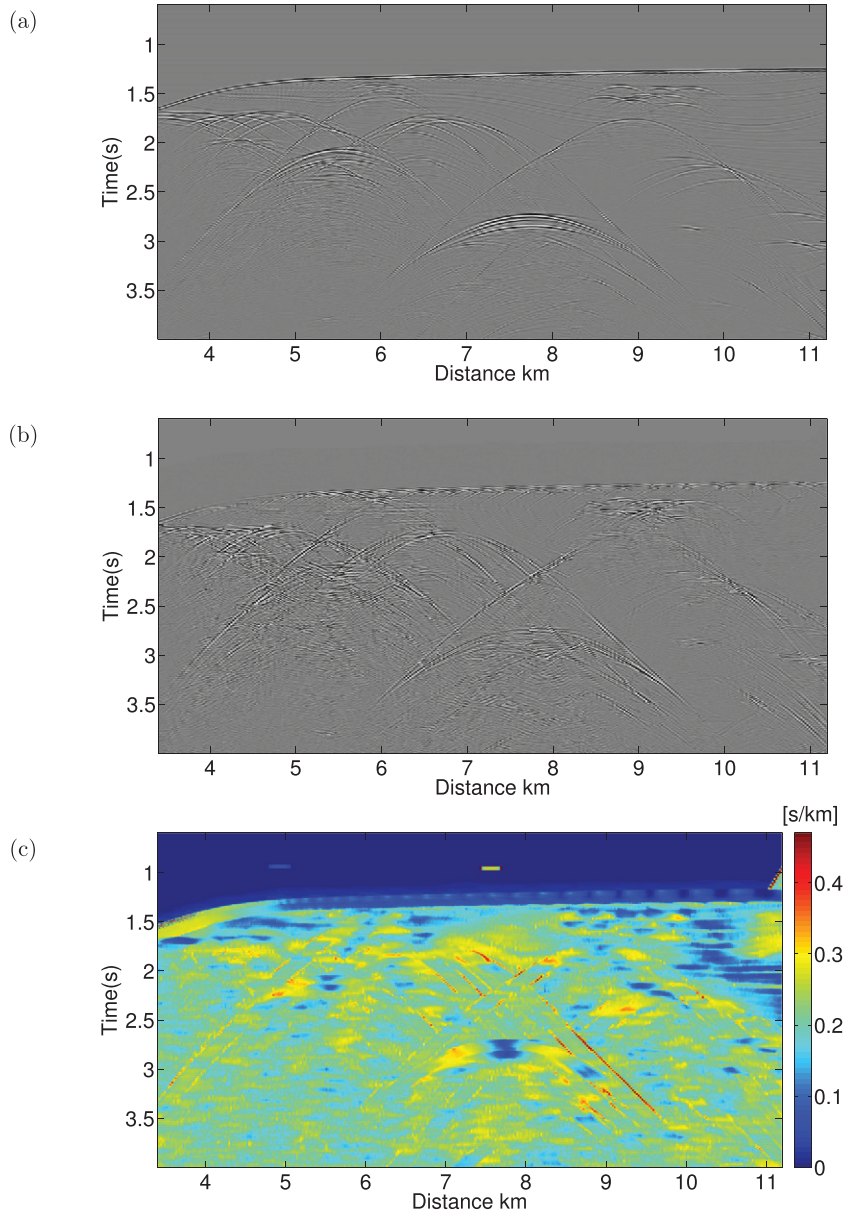

Figure 1. (a) Near-offset section from the Sigsbee2B synthetic dataset. (b) Same near-offset section after plane-wave destruction. (c) Local slopes panel.

To better understand the performance of the PWD filter, we tested it on synthetic data before applying it to the real dataset. Figure 1 compares the original near-offset section (part a) from the Sigsbee2B dataset to the one after application of the PWD filter implemented this work (part b). Figure 1(c) shows the panel of local slopes estimated from the near-offset section in part (a). We recognize that the suppression of reflected energy by means of our PWD filter is far from perfect. However, the reflection events have been sufficiently reduced for diffraction events to become visible.

RDM analysis

The main purpose of our work is to test the residual-diffraction-moveout migration-velocity-analysis method of Coimbra *et al* (2013) on real data. The method is based on the localization and picking of the residual moveout of incorrectly migrated diffraction events in depth domain. Here, we applied the methodology to construct velocity models in both the depth and the time domain.

Following Coimbra *et al* (2013), we consider a diffraction point at the true position (x_t, z_t) in a constant-velocity medium with true velocity v_t. Then, according to Hubral *et al* (1996), the residual moveout of a diffraction event after of depth migration with an incorrect velocity v_0 coincides with the position of the Huygens image-wave for the depth remigration from velocity v_t to v_0, defined as the curve or surface of all points where a possible event at the image point (x_t, z_t) might be placed when the migration velocity is changed from v_t to v_0. That is, if the migration velocity is higher than the medium velocity, the overmigrated diffraction events will have the shapes of ellipses or if the migration velocity is smaller, the shapes of the undermigrated diffraction events are hyperbolas. Hubral *et al* (1996) show that the position of the Huygens image-wave is given by

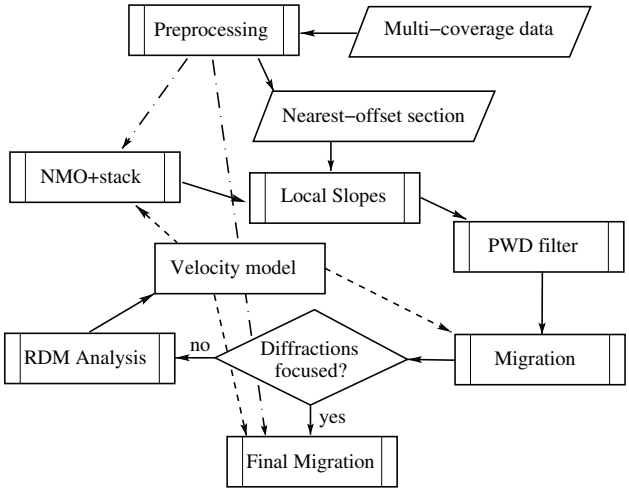

Figure 2. The flowchart of RDM processing on real data. Solid arrows show the actual flow, dashed arrows indicate auxiliary information, dash–dotted arrows represent the use of the preprocessed data at later stages of the process.

$$\frac{z^2}{v_0^2} + \frac{(x - x_t)^2}{v_0^2 - v_t^2} = \frac{z_t^2}{v_t^2}. \tag{6}$$

However, the preferred parameters to describe a hyperbola or an ellipse are the half-axes (a and b). Therefore, Coimbra *et al* (2013) rewrite equation (6) in the form

$$\frac{z^2}{b^2} + s\frac{(x - x_t)^2}{a^2} = 1, \tag{7}$$

where the half-axes a and b are given by,

$$a = \frac{z_t}{v_t}\sqrt{|v_0^2 - v_t^2|} \quad \text{and} \quad b = \frac{z_t}{v_t}v_0. \tag{8}$$

Depending on the sign $s = \text{sgn}(v_0^2 - v_t^2) = \text{sgn}(v_o - v_t)$, equation (7) can represent an ellipse or a hyperbola.

Under the assumption that below a sufficiently well-known overburden, the diffraction events locally behave in the same way as in a homogeneous medium, Coimbra *et al* (2013) used a least-squares method to find the best-fitting hyperbola to describe an undermigrated diffraction event or the best-fitting ellipse for an overmigrated diffraction event. This provides an estimation for the half-axes a and b as well as the horizontal coordinate of the apex x_t. In other words, the a and b parameters are related to the residual moveout of an incorrectly migrated diffractions.

In a medium with a strong velocity gradient, the positioning of the hyperbola or ellipse can be strongly affected. For that reason, Coimbra *et al* (2013) work with a modified version of equation (7), being

$$\frac{z^2}{b^2} + s\frac{(x - x_t)^2}{a^2} = 1 + \epsilon(x - x_t)z, \tag{9}$$

where $\epsilon(x - x_t)z$ is a mixed perturbation term that allows for a rotation of the ellipse or hyperbola. The parameter ϵ is adjusted together with the other parameters in the least-squares procedure.

Then, Coimbra *et al* (2013) show how this information on the residual moveout of the incorrectly migrated diffraction events can be used to update the migration velocity model in two different ways. One of them makes direct use of the half-axes and the other one traces remigration trajectories. In this work, we use the latter technique. As defined by Hubral *et al* (1996), remigration trajectories are ray-like solutions to the remigration image-wave equation. These remigration trajectories connect all possible positions where a diffraction event can be found in a migrated image as a function of migration velocity. More detail about the RDM method can be found in Coimbra *et al* (2013), who demonstrated a successful application of the technique to the Sigsbee2B data.

In this work, we apply the RDM technique to real data from the Viking Graben. However, in real data, the identification of diffraction events is rather difficult. The energy difference between reflections and diffractions is very large. Moreover, noise may distort the information. Therefore, it is easy to select an incorrect event, in the believe that is a diffraction event. Therefore, we apply the described suppression of reflections before trying to interpret the diffractions. As we will see below, incomplete suppression of the reflected energy turns out to be sufficient for our purposes. Since the RDM technique is an iterative and quite fast procedure, possible errors (for example due to incorrect selection of an event or bad fit of an ellipse or hyperbola) at one iteration can be corrected for in the next iteration.

RDM processing steps

The RDM processing sequence consists of the following steps:

- (1) Preprocessing (geometry correction, trace editing, deconvolution, band-pass filtering and AGC) of the real data set. This preprocessing was performed in the same way for both the conventional and unconventional velocity analyses.
- (2) Selection of the nearest-offset gather from the real data set.
- (3) Local-slope estimation in the selected section.
- (4) Application of the PWD filter to suppress reflected energy.
- (5) Migration of filtered section (constant velocity model, for example $v = 1500$ m s^{-1}, in the first iteration, then model resulting from the previous iteration).
- (6) Velocity-model update using RDM processing.
- (7) NMO+stack using this velocity model on the full data set to obtain an improved zero-offset section.
- (8) Iteration of steps (3)–(7) until the diffractions are focused.

Figure 2 shows a flowchart of the procedure.

In our application of the above processing sequence to the Viking Graben dataset, only two iterations were necessary for convergence. Other data may require more than two iterations to achieve a reasonable velocity model for migration. In other words, we expect the number of iterations required to depend on the complexity of the data.

Numerical results

The objective of this work was to extract a velocity model from real data using the RDM technique. Our test data set is a Viking Graben dataset from the North Sea Basin provided

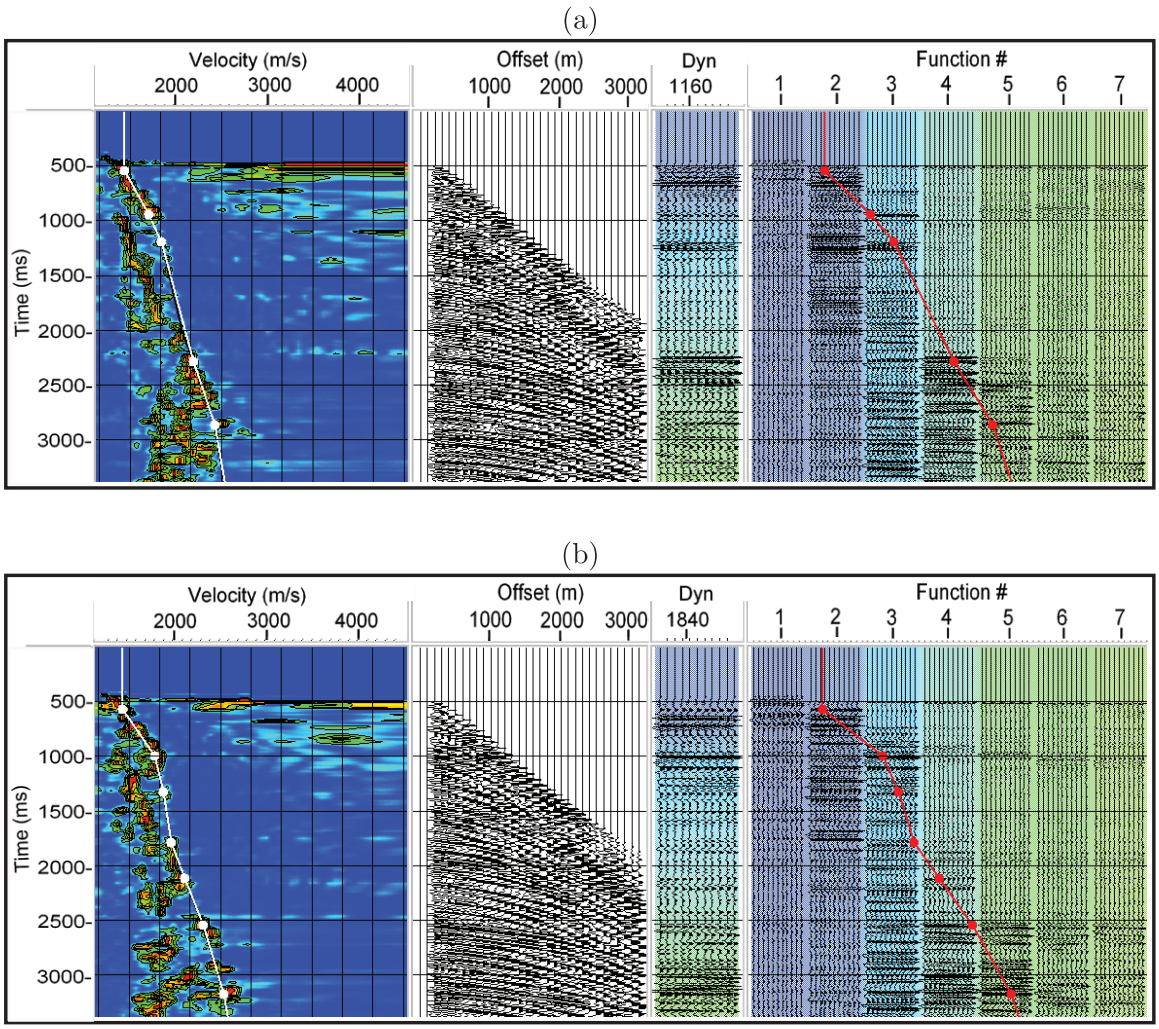

Figure 3. Conventional velocity analysis at (a) CMP 1163 and (b) CMP 1843.

by ExxonMobil. Because of a large number of diffractions, this data set is well-suited for an application of the RDM method. One should keep in mind that to successfully apply this method, the data must contain many diffractions. In geological terms, this means that there are many faults and discontinuities in the subsurface.

Dataset description and preprocessing

The Viking Graben data set was acquired with 1001 shot points and 120 channels. The sampling rate was 4 ms and the recording time was 6 s. The distances between the shot points and also between the receivers were 25 m. The minimum and maximum offsets were 262 m and 3237 m, respectively. The water depth along the seismic line was about 300 m with very little variations.

The data set needed seismic preprocessing to enhance the data and to attenuate the noise before applying our methodology. The preprocessing and processing steps consisted of: trace muting, bandpass filtering with a zero-phase (6–12–50–70) Hz Ormsby filter, spherical divergence corrections, and predictive deconvolution with an operator length of 320 ms and a 20 ms prediction operator. We also used a deconvolution with white noise ($S/N = 0.1$) and a predictive deconvolution to improve the amplitude resolution. The preprocessing as well as all post-stack time and depth migrations were carried out with conventional tools.

NMO velocity analysis

As a reference, we performed conventional CMP processing of the Viking Graben data set to obtain post-stack time and depth-migrated images and the corresponding velocity models for a comparison with the results from the RDM method (as mentioned before, we call this procedure RDM processing). To compare with other seismic images of the Viking Graben, we used the time-migrated image of Gislain and McMechan (2003).

We performed a CMP velocity analysis at every 50 midpoints using velocity spectra ranging from 1500 m s^{-1} to 3000 m s^{-1}. Figure 3 shows the semblance velocity analysis at CMPs 1163 and 1843. We then interpolated these velocity data to construct a velocity model used in the normal-moveout (NMO) correction and stack. We then performed a second velocity analysis to improve the NMO correction. Figure 4 shows the resulting RMS velocity model and figure 5 depicts the NMO-stacked section from this processing.

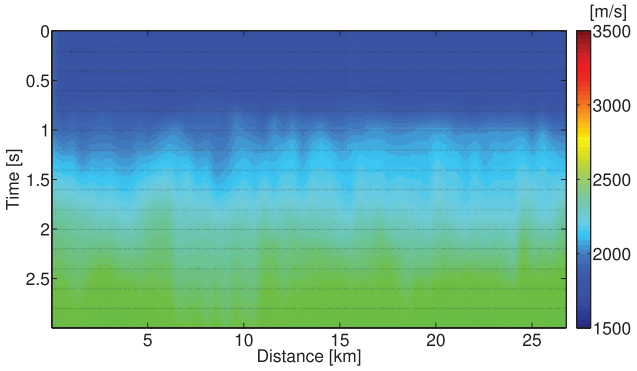

Figure 4. RMS velocity model from CMP processing.

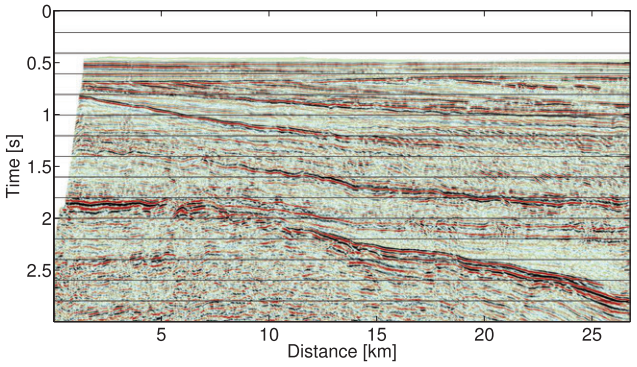

Figure 5. NMO stacked section from CMP processing.

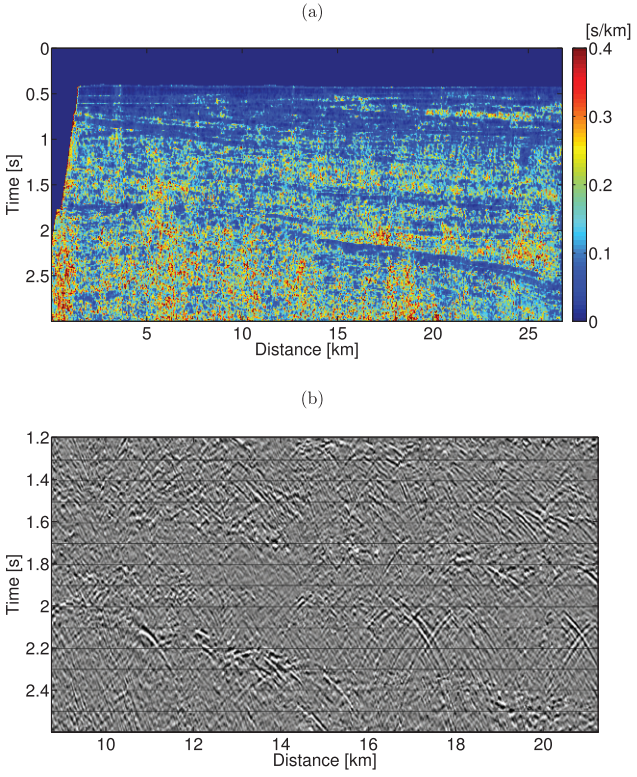

Figure 6. Application of the PWD filter. (a) Local slopes extracted from the NMO-stacked section. (b) PWD-filtered NMO-stacked section (central part).

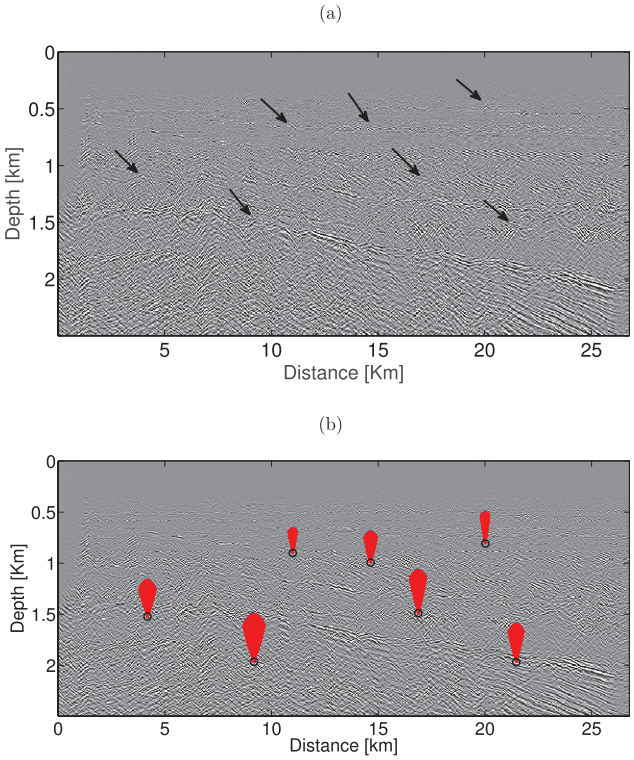

Figure 7. RDM method applied to the NMO-stacked section. (a) Image after depth migration with water velocity $v_0 = 1500$ m s^{-1}. Notice several undermigrated diffraction (arrows). (b) Remigration trajectories (red lines forming cones) starting at seven of the undermigrated diffractions.

RDM application on the NMO-stacked section

Since the RMD method theoretically requires a zero-offset section as its input, we applied it as a first test to the NMO-stacked section obtained from CMP processing. In this way, we were trying to assess whether the RDM method can extract velocity information from real data. From a successful application, we are also able to update the velocity model and make it more suitable for a post-stack time migration.

In order to make the diffraction events better interpretable in the NMO-stacked section, we reduced the reflected energy. For that purpose, we first estimated the local slopes in that section (see figure 6(a)). We then attenuated the energy in the slope direction using a PWD filter as described above. Figure 6(b) shows the central window of the resulting PWD-filtered NMO-stacked section. We can clearly see that the diffraction events are now much better visible. In this way, they will become interpretable in the migrated section.

As previously mentioned, the RDM methods consists of the interpretation of unfocused diffraction events in the migrated depth domain. In the same way as Coimbra *et al* (2013) did for the Sigsbee2B data, we initiated the process with a constant-velocity migration. We performed a depth Kirchhoff migration of the diffraction-enhanced NMO-stacked section using the water velocity $v_0 = 1500$ m s^{-1}. Figure 7(a) shows the central part of the resulting migrated image from 0.8 to 2 km in depth and from 8 to 22 km in the distance. We recognize a number of undermigrated diffractions.

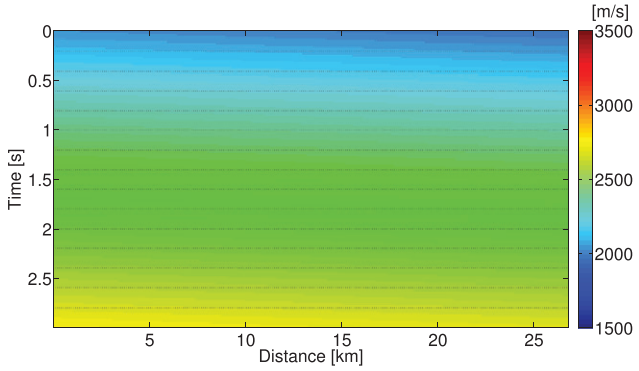

Figure 8. The RMS velocity model from RDM processing applied on ZO section.

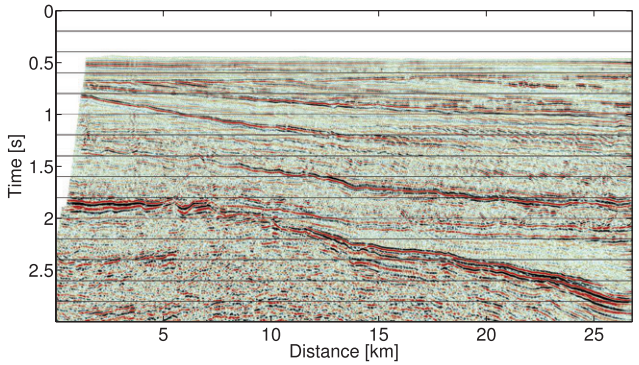

Figure 9. The time migration section from RDM processing applied on ZO section.

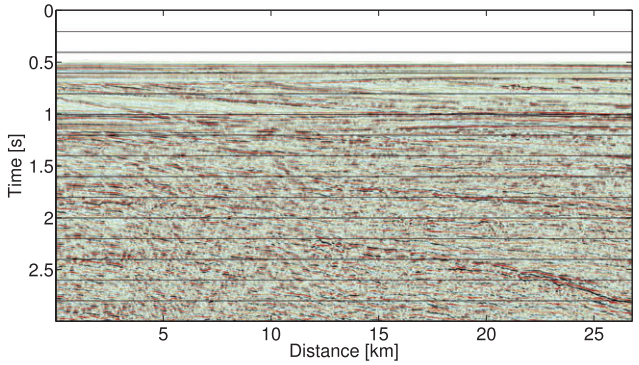

Figure 10. Nearest-offset section of the Viking-Graben data set. This was the input to the first iteration of RDM processing.

This depth section was the input to the RDM method. We adjusted hyperbolic arcs to seven identified diffraction events and traced remigration trajectories starting at those arcs. Figure 7(b) shows in red the cones formed by the (densely sampled) remigration trajectories. Also indicated by black circles are the focusing points of these trajectories. The velocity updates resulting from the procedure are applied at these points.

From the updated velocity at the seven focus points, together with setting the velocity to water velocity at the top of the model, we generated a new velocity model by means of B-splines interpolation. To test its quality, we converted it to a time-domain RMS velocity model (figure 8) and used it to time-migrate the unfiltered NMO-stacked section. The result is shown in figure 9. We see that the obtained time-migration

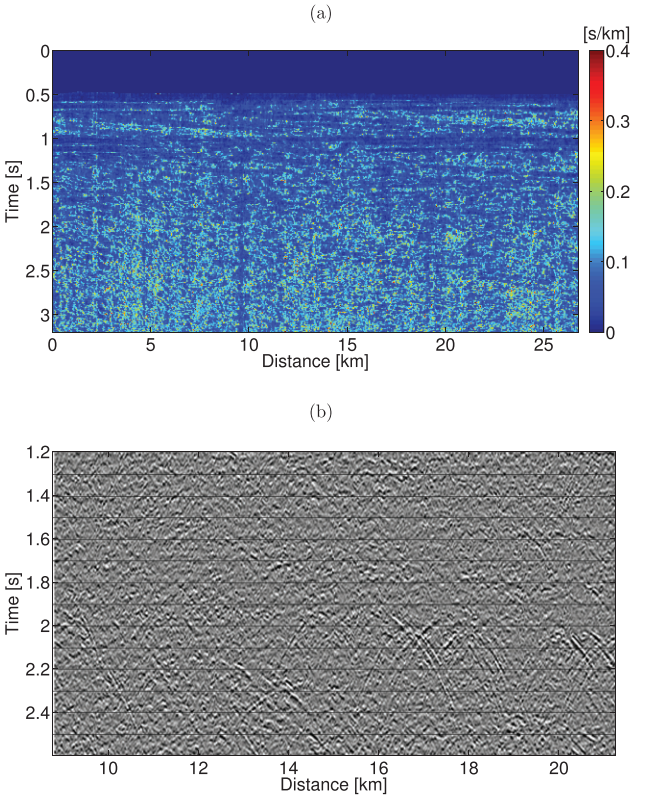

Figure 11. First iteration of RDM processing. (a) Local slopes of the nearest-offset section. (b) Central part of the PWD-filtered section. The window ranges from 8 km to 22 km horizontally and from 1.2 s to 2.6 s in time.

velocity model is already of sufficient quality to reasonably focus the reflection events (which where not used at all to generate the model).

This result is important, because it demonstrates that the RDM method can be used to extract velocity information from real data. It is instructive to note that no perfect separation of diffraction and reflection events was necessary to apply the RDM method. All that was needed was the interpretability of the migrated diffractions. The fact that the regions of the apices of most diffractions were attenuated together with the reflections (see again figure 6(b)) was also no obstacle to the velocity-updating procedure.

However, the procedure described in this section still relied on a previous NMO velocity analysis. Therefore, it is not clear how much velocity information was carried over to the RDM analysis. To evaluate if the RDM method can be applied on its own, we started the procedure all over, initiating with the nearest-offset section in the data instead of an NMO-stacked section. In this way, the result will depend only on velocity information extracted from the diffraction events without help from any other source.

RDM processing of a near-offset section

The same processing sequence as detailed in the previous section was required to apply the residual-diffraction-moveout migration-velocity analysis of Coimbra *et al* (2013) directly to a near-offset section of our real data set. The careful application

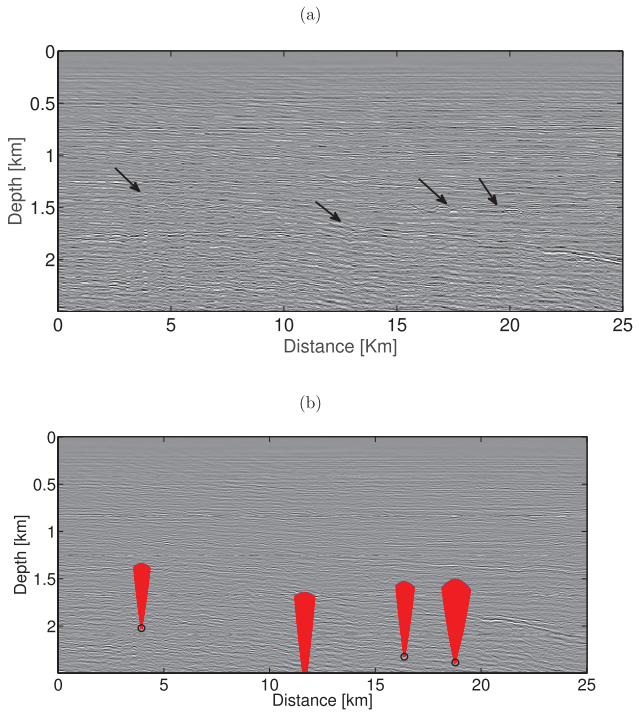

Figure 12. First iteration of RDM processing. (a) Depth migrated image of PWD-filtered section. Initial velocity model is water velocity $v_0 = 1500$ m s^{-1}. (b) Interpreted diffraction events with remigration trajectories (red lines forming cones) and their focusing points (black circles).

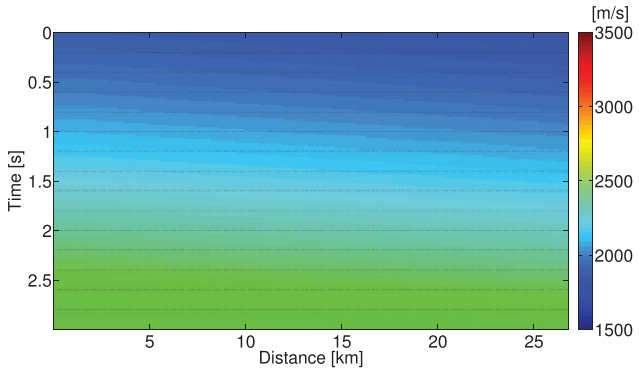

Figure 13. RMS velocity model from first iteration of RDM processing.

of all processing steps was fundamental to achieving good results. Therefore, we refer to this processing sequence, consisting of local-slope estimation, PWD filtering, and iterative diffraction-moveout analysis, as RDM processing. As we will see below, the application of these RDM processing steps provided acceptable velocity models in the time and depth domains.

First iteration. Theoretically, the RDM method requires a zero offset (ZO) section as input (Coimbra *et al* 2013). In real data, a zero-offset section is not available. Therefore, a straightforward idea is to use an existing near-offset section in the hope that the small deviation from a zero-offset section is negligible. It can be expected that possible errors should occur mainly in the shallow parts of the model, and that such errors will be corrected in subsequent iterations of the method.

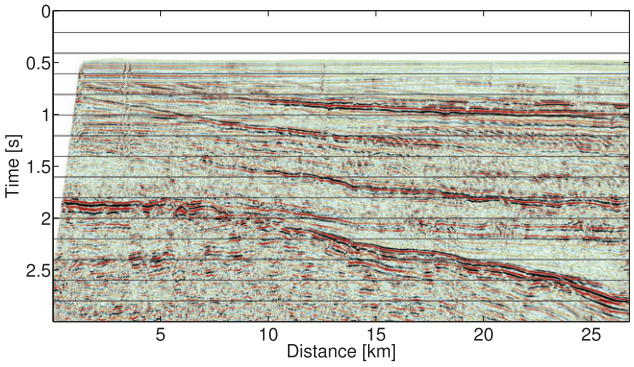

Figure 14. NMO-stacked section from first iteration of RDM processing. This section is constructed using the velocity model from the first iteration and will be the input to the second iteration.

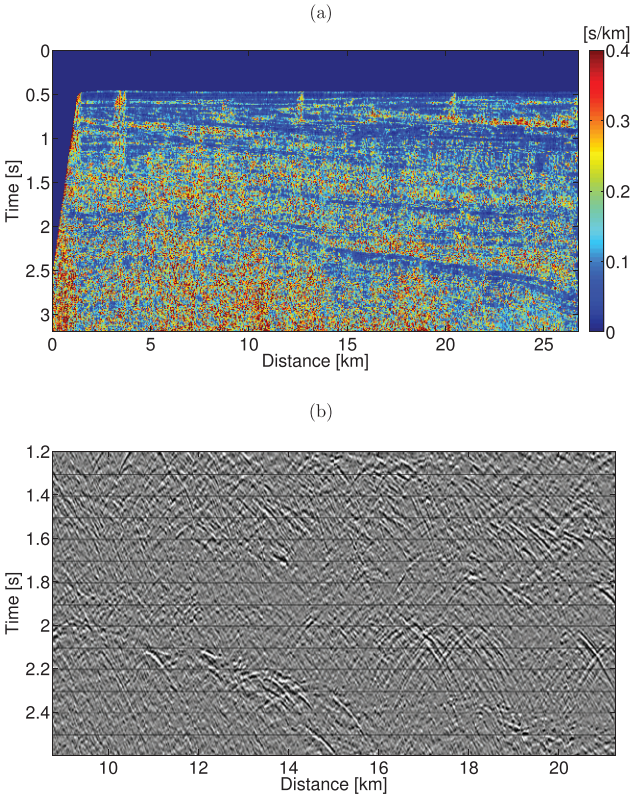

Figure 15. Second iteration of RDM processing. (a) Local slopes from NMO-stacked section after the first iteration. (b) PWD-filtered section with visible unfocused diffraction events.

In the Viking Graben data set, the nearest-offset section corresponds to a source-receiver offset of 262 m. Figure 10 shows this nearest-offset section, which we used as the input data to the first iteration of the RDM method. For subsequent iterations, the input was the NMO-stacked section obtained with the velocity model from the previous iteration.

Of course, in the unfiltered near offset section, it is difficult to identify the diffraction events (see figure 10). Therefore, we had to start the procedure again by applying the PWD filter. Figure 11(a) shows the local slopes extracted from the nearest-offset section. Even though there is little variation in the slope values, we can recognize the smaller slopes of a number of reflection events. These events are then suppressed in the PWD-filtered section. Particularly in its central part

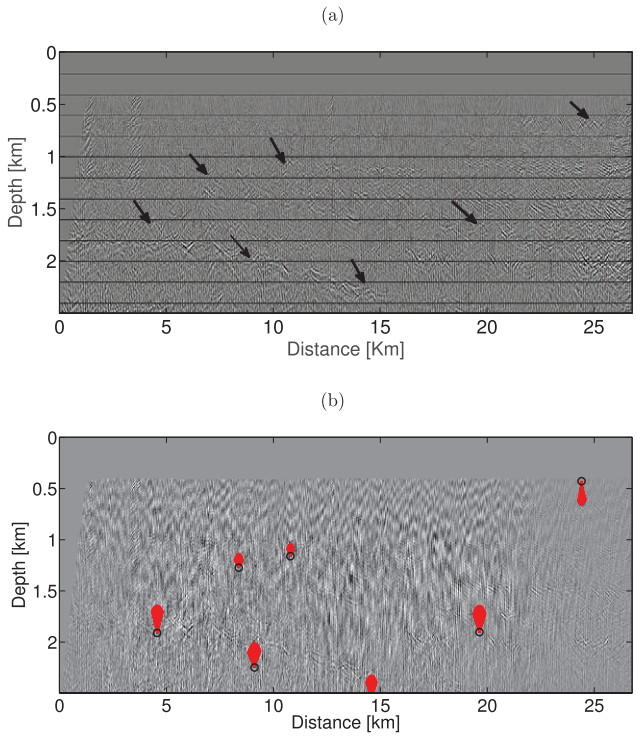

Figure 16. Second iteration of RDM processing. (a) Depth-migrated of PWD-filtered section. The migration was done with the velocity model from the first iteration. (b) Unfocused diffraction events with remigration trajectories (red lines) and their focus points (black circles).

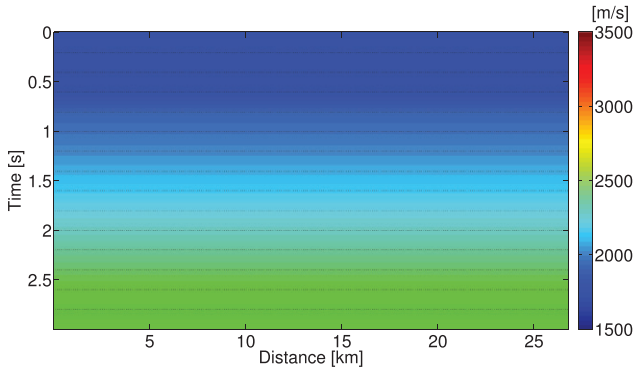

Figure 17. RMS velocity model from second iteration of RDM processing.

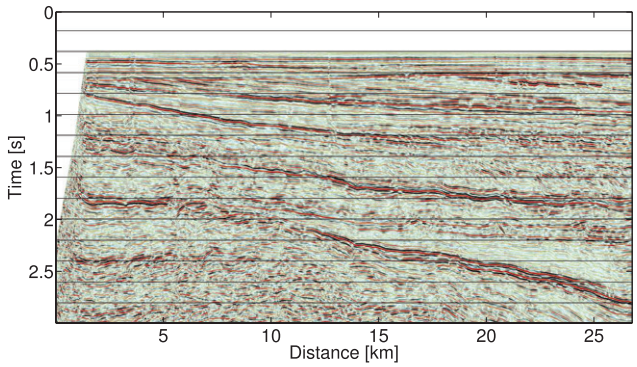

Figure 18. NMO-stacked section from second iteration of RDM processing.

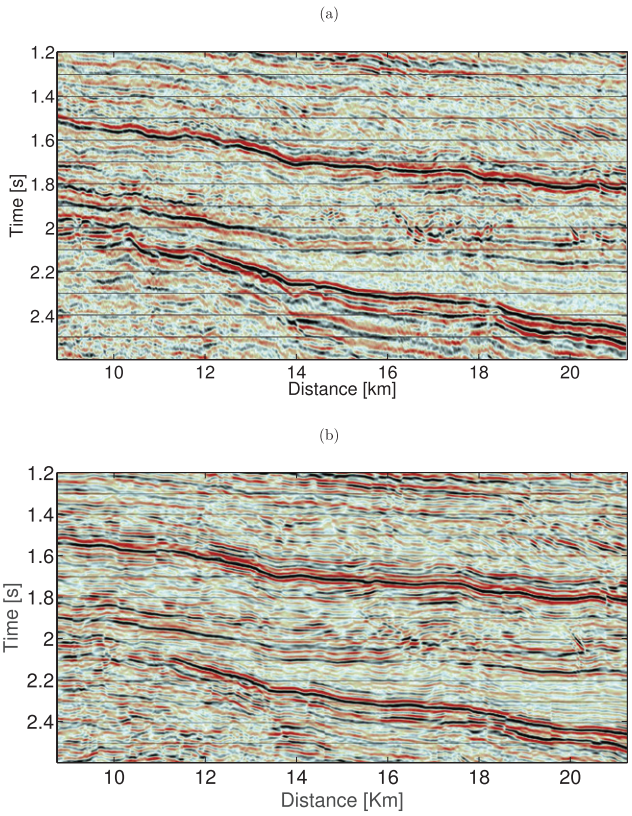

Figure 19. Time migrated sections with the velocity models from (a) CMP processing and (b) RDM processing. The images were windowed horizontally (from 0.8 to 22 km) and in time (from 1.2 to 2.6 s) for better visualization.

(figure 11(b)), several diffraction events have become visible, permitting their interpretation after migration.

Following the RDM processing sequence detailed above, we next performed a depth Kirchhoff migration on the PWD-filtered section, using water velocity ($v_0 = 1500$ m s^{-1}). The result, shown in figure 12(a), exhibits several undermigrated diffraction events in the depth domain. To better visualize the diffractions, we windowed the migrated image from 0.8 to 2 km in depth and from 8 to 22 km in distance. Figure 12(b) shows four interpreted diffraction events together with their remigration trajectories (red lines), used to update the first velocity model. Again, the velocity at the top of the model was held constant at water velocity.

With the updated RMS velocity model (figure 13), we applied the NMO correction and stacked the result to obtain a first stacked zero-offset section (figure 14), which is the input to the second iteration. As we can see, the reflectors on the left-hand side of figure 14 are not well focused. This happened because we did not find interpretable diffractions in these regions in the first iteration. However, as we will see below, the information carried over from farther-away diffractions helped to update the model sufficiently so that some diffractions can be interpreted in the second iteration.

Second iteration. Since there is room for improvement in the NMO-stacked section of figure 14, we used it as an input to a second RDM iteration. Figure 15(a) shows the local slopes estimated from this section. We see the improvement in the

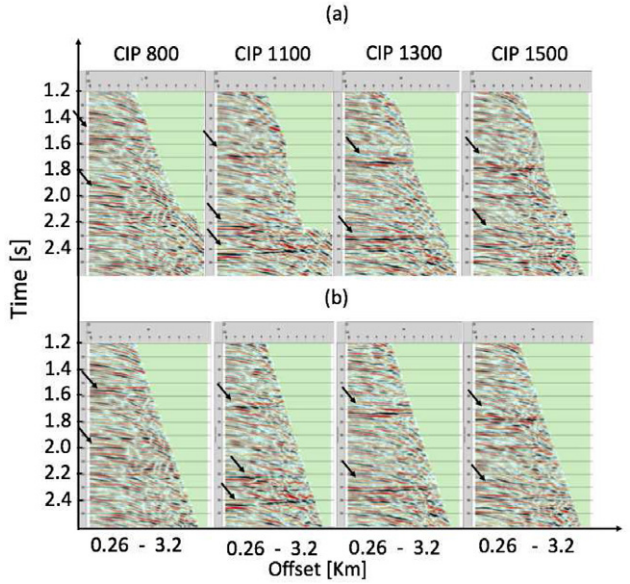

Figure 20. Time-migrated common image point (CIP) gathers at CMPs 800, 1100, 1300 and 1500 using the velocity models from (a) conventional processing and (b) RDM processing.

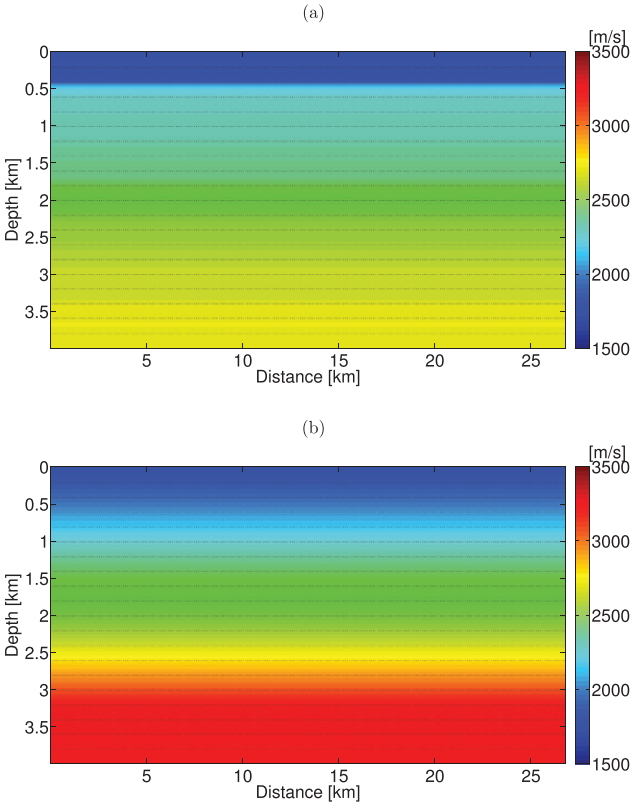

Figure 21. Final depth velocity models. (a) CMP processing and Dix inversion. (b) RDM processing and average-slowness inversion.

slopes of the reflectors as compared to the ones of the first iteration (see again figure 11(a)). Therefore, the suppression of reflections is more effective, resulting in the visibility of some additional diffraction events, particularly in the left part of the section (see figure 15(b)). This will help us to further improve the velocity model generated in the first iteration.

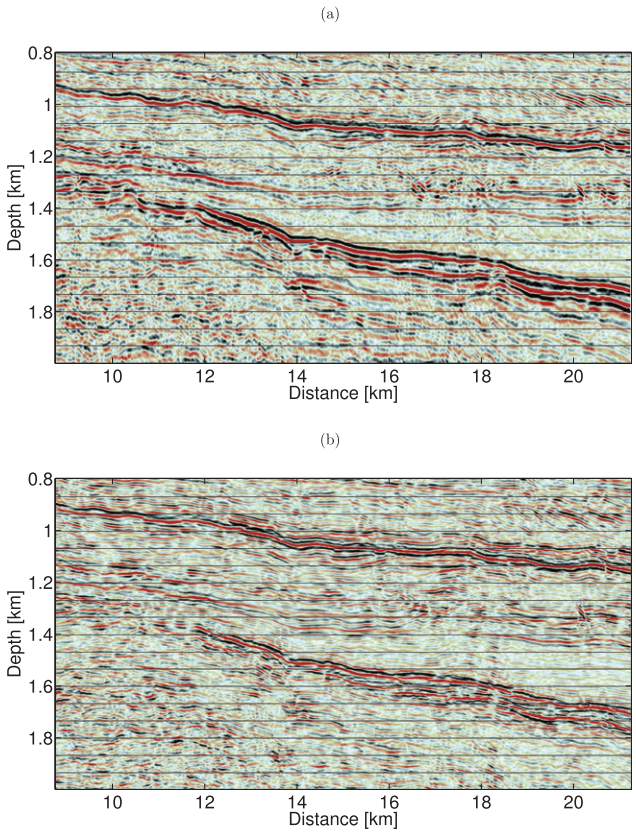

Figure 22. Depth migration sections using interval velocity model from (a) conventional processing and (b) RDM processing. The images were windowed horizontally (from 0.8 to 22 km) and in depth (from 1.2 km to 3.0 km).

From the second iteration on, each depth migration of the diffraction panel is performed with the velocity model found in the previous iteration. Figure 16(a) shows the central part of the PWD-filtered section after Kirchhoff depth-migration with the velocity model from the first iteration. In figure 16(b) we see interpreted one overmigrated and six undermigrated diffraction events together with remigration trajectories and their focus points.

The same velocity-model updating procedure as before, using the velocity information at these focus points, yields the new RMS velocity model of figure 17. Using this velocity model, we obtained a new NMO-stacked section (figure 18). The continuity of the shallow reflectors has been greatly improved over the first stack (see again figure 14). This indicates that the velocity model has improved in this region, as expected. The error in the shallow part in the first iteration can be attributed to our use of a near-offset section to approximate a zero-offset section. On the other hand, the reflector slightly above 2 s seems to have lost focus. This might have been improved with another iteration.

Comparison of CMP and RDM results

After establishing the velocity models in the time and depth domains using velocity analyses by means of CMP and RDM processing, we performed a post-stack Kirchhoff migration in the time and depth domains. In both cases, we used

a maximum frequency of 50.0 Hz for migration. All other parameters except for the velocity models were kept the same.

Time migration. Figure 19 shows the central parts of the post-stack time migrated sections. As can be noted, the results are quite similar. However, closer inspection reveals some differences. The time migrated image using the velocity model from CMP processing (figure 19(a)) shows stronger reflectors in the deeper part. However, the local lateral variations of the reflectors are slightly wrong, and the events below 2.2 s and in the first 12 km have low coherence. In contrast, the time migration with the RDM velocity (figure 19(b)) shows a good energy distribution with a smooth local lateral variation. The dipping reflector at the top of the model present better continuity and the reflections in the lower left corner below 2.2 s are better imaged. However the event starting at 2 s on the left-hand side is less visible. For a comparison with results from independent processing, the reader is referred to Gislain and McMechan (2003).

Figure 20 shows the common image point (CIP) gathers at CMP locations 800, 1100, 1300 and 1500 as obtained from time migration using the conventional and RDM velocity models. These locations correspond to distances 10, 13.75, 16.25 and 18.75 km in the migrated images in figure 21. We note very similar flattening behavior of the principal events (see arrows) in the CIP gathers for both velocities models, indicating that the two models are of similar quality.

Depth migration. The theory of the RDM method is based on the remigration image-wave equation (Hubral *et al* 1996), which relies on average velocities. As shown by Schleicher *et al* (2004) these average velocities correspond to mean slownesses. Based on this observation, Coimbra *et al* (2013) developed a procedure to convert the RDM average velocities into interval velocities that can be used for depth migration.

Figure 21 shows the depth velocity models from CMP and RDM processing. The average velocity from the RDM method was converted for interval velocity the procedure of Coimbra *et al* (2013). The interval velocity from CMP processing was obtained by means of Dix inversion (by PROMAX). In both cases, no lateral variations are taken into account. However, the velocity from RDM processing has a better correlation with layers in the seismic section than the conventional velocity. Another difference is the value of the velocity at the depths greater than 2 km. It can be noted that the velocity increase with depth is stronger in the RDM model than in the conventional velocity model. This behavior has an effect on the position of the reflectors in depth migration. The conventional model can be enhanced to find a better correlation with the layers, but that will require more run time as compared with RDM processing.

With the velocity models in the depth domain from the RDM and CMP processing, we performed Kirchhoff depth migrations (figure 22). The main difference between the migrated images lies in the position of the reflectors in depth. The RDM velocity model consistently places all of them at shallower depths. On the left-hand side, the CMP-processed image (figure 22(a)) seems to slightly better focus the reflector at about 1.3 km depth, but in the RDM-processed image (figure 22(b)), weak reflectors at 1.6 km and 1.8 km depth come into focus that are barely visible in the CMP-processed image. Moreover, the two faults at about 13.8 km and 14.6 km distance are much more easily interpretable in the RDM-processed image (figure 22(b)).

Overall, the general impression is that both images could benefit from further improvements, but that they are of comparable quality. It is to be kept in mind in this respect that the RDM processing was much faster and less expensive than the CMP processing.

Note that the main goal of this work is to demonstrate that velocity information can be extracted from real data by means of the RDM method, and that this information can be used to to improve velocity models in the time and depth domains. It is very probable that some parameters can be better adjusted for both the CMP and RDM processing sequences to come up with better results. Further tests are required with other methods for local slope estimation, suppression of reflection events, or velocity interpolations to determine the full potential of the RDM method. Also, its use for local improvements of an *a priori* velocity model, particularly to better focus a target below a reasonably well-known overburden must be further investigated.

In this simple test on a real data set, the application of RDM was considerable faster than CMP processing due the small number of picked diffraction points (eleven) required to reach an acceptable velocity model. However, in a complex data set or 3D data, the manual picking may become very costly. In this situation automatic diffraction picking should be considered in order to keep the procedure feasible.

Conclusions

In this paper, we have applied the residual-diffraction-moveout migration-velocity-analysis technique of Coimbra *et al* (2013) to a real data set from the Viking Graben. To assess the quality of the method we have compared the seismic migrated images obtained by standard CMP processing with migrated images obtained by a new processing sequence that uses the RDM technique. Although this technique had been theoretically developed for zero-offset sections, the error produced in applying the method to a near-offset profile was overcome in a second iteration. We have shown here that for near offset sections from Viking Graben seismic data, only two iterations were sufficient to overcome the near offset problem and produce acceptable velocity models for time and depth migration.

To be able to interpret the uncollapsed diffraction events in the migrated sections, we have used a PWD filter to attenuate the reflected energy. This filter was an essential step in the RDM

processing sequence, in view of the weak energy of diffractions as compared with the energy of reflections and sometimes even the noise. It is important to note that it was not necessary to perfectly suppress all reflected energy in order to make the diffractions interpretable. Moreover, though the PWD filter sometimes suppressed the apexes of the uncollapsed diffraction events, they could still be used for velocity analysis.

The velocity models in the time and depth domains obtained from RDM processing produced acceptable seismic images that were comparable to the ones obtained through standard CMP processing. The important difference between the methods was the time it took to construct the velocity models. The time spent to achieve an acceptable migration-velocity model was significantly less using RDM processing than CMP processing. For the Viking Graben data set, we were able to produce a satisfactory migration-velocity model in a single day, while the CMP analysis took four days.

It is important to emphasize that we do not aim at suggesting that the RDM methodology is better or worse than any conventional methodologies. Our purpose is to test an additional tool for velocity-model building that directly uses the velocity information contained in diffractions. It should be noted that by applying the method without an initial model, we have subjected it in this work to the hardest possible test. Another, possibly even more valuable application is to assess and improve the quality of an already available *a priori* velocity model. In this way, even more unfocused diffractions might become visible and interpretable. While with our Viking-Graben real-data example, we have shown its exclusive use from scratch, we feel that its true potential lies in achieving local improvements of previous velocity models above or at the target.

As commented by Coimbra *et al* (2013), the most attractive feature of the RDM method is its low computational cost. The principal computational cost of the RDM method lies in the intermediate migrations at each iteration. Since these are zero-offset migrations, though, this is rather inexpensive as compared to other MVA techniques. Of course, it is hard to quantify the seismic processing time, especially when the time heavily depends on human interaction. In our example, most of the time required to reach an applicable velocity model was spent on identifying the diffractions. Here, the plane-wave-destruction filtering turned out to be crucial to help the interpreter see diffraction events. If the diffraction picking can be automatized (see de Figueiredo *et al* 2013, for some ideas), possibly with an improved attenuation of reflections, the RDM method should be a very cheap method to construct or at least improve a velocity model.

Acknowledgments

The authors would like to thank reviewer Mamoru Takanashi for his helpful remarks. Moreover, we are grateful to ExxonMobil for providing the Viking Graben data set. This work was kindly supported by the Brazilian agencies CAPES, FINEP, and CNPq, as well as Petrobras and the sponsors of the Wave Inversion Technology (WIT) Consortium.

References

Alonaizi F, Pevzner R, Bóna A, Alshamry M, Caspari E and Gurevich B 2014 Application of diffracted wave analysis to time-lapse seismic data for CO_2 leakage detection *Geophys. Prospect.* **62** 197–209

Alonaizi F, Pevzner R, Bóna A, Shulakova V and Gurevich B 2013 3D diffraction imaging of linear features and its application to seismic monitoring *Geophys. Prospect.* **61** 1206–17

Asgedom E G, Gelius L J and Tygel M 2011 Diffraction separation using the CRS technique: a field data application *12th Int. Congress of the Brazilian Geophysical Society & EXPOGEF* pp 976–9

Claerbout J F 1992 *Earth Soundings Analysis—Processing Versus Inversion* (Oxford: Blackwell)

Coimbra T A, de Figueiredo J J S, Schleicher J, Novais A and Costa J C 2013 Migration velocity analysis using residual diffraction moveout in the poststack depth domain *Geophysics* **78** S125–35

de Figueiredo J, Oliveira F, Esmi E, Freitas L, Schleicher J, Novais A, Sussner P and Green S 2013 Automatic detection and imaging of diffraction points using pattern recognition *Geophys. Prospect.* **61** 368–79

Dell S and Gajewski D 2011 Common-reflection-surface-based workflow for diffraction imaging *Geophysics* **76** S187–95

Fomel S 2009 Applications of plane-wave destruction filters *Geophysics* **67** 1946–60

Fomel S, Landa E and Taner M T 2007 Post-stack velocity analysis by separation and imaging of seismic diffractions *Geophysics* **72** U89–94

Gislain B M and McMechan G A 2003 Processing, inversion, and interpretation of a 2d seismic data set from the north viking graben, north sea *Geophysics* **68** 837–48

Hubral P, Tygel M and Schleicher J 1996 Seismic image waves *Geophys. J. Int.* **125** 431–42

Khaidukov V, Landa E and Moser T J 2004 Diffraction imaging by focusing–defocusing: an outlook on seismic superresolution *Geophysics* **69** 1478–90

Klokov A and Fomel S 2013 Separation and imaging of seismic diffractions using migrated dip-angle gathers *Geophysics* **77** S131–43

Landa E and Keydar S 1998 Seismic monitoring of diffraction images for detection of local heterogeneities *Geophysics* **63** 1093–100

Landa E, Fomel S and Reshef M 2008 Separation, imaging, and velocity analysis of seismic diffractions using migrated dip-angle gathers *79th Annual Int. Meeting, SEG, Expanded Abstracts* pp 2176–80

Landa E, Shtivelman V and Gelchinsky B 1987 A method for detection of diffracted waves on commom-offset sections *Geophys. Prospect.* **35** 359–74

Liu T, Hu J and Wang H 2013 Diffraction wavefield separation and imaging using singular spectrum analysis *78th EAGE Conf. and Exhibition Incorporating SPE EUROPEC* pp 10–3

Novais A, Costa J and Schleicher J 2008 GPR velocity determination by image-wave remigration *J. Appl. Geophys.* **65** 65–72

Sava P, Biondi B and Etgen J 2005 Wave-equation migration velocity analysis by focusing diffractions and reflections *Geophysics* **70** U19–27

Schleicher J, Costa J C, Santos L T, Novais A and Tygel M 2009 On the estimation of local slopes *Geophysics* **74** 25–33

Schleicher J, Novias A and Munerato F 2004 Migration velocity analysis by depth image-wave remigration: first results *Geophys. Prospect.* **52** 559–73

Zhang R 2004 Imaging the earth using seismic diffractions *Annual Report from Consortium for the Development of Specialized Seismic Techniques* pp 1–41